Bulletin of the
Mineral Research and Exploration

GEOPHYSICAL ANALYSIS AND MODELLING OF THE SİMAV BASIN, WESTERN ANATOLIA

Ceyhan Ertan TOKER[a]

[a] MTA Genel Müdürlüğü Jeofizik Etütler Daire Başkanlığı, Ankara, Turkey

ABSTRACT

The various data processing techniques, to illuminate the parameters of the geological structure which are applied in gravity and magnetic potential field methods. Also edge detection procedures are in data processing techniques. In this study, 2D, 3D, inversion and asta technique is one of the new edge detection procedures were applied to clarify correlation between the Simav half graben's deep position and geometry of the tectonic lineaments. The Asta is obtained using the tilt angle.

1. Intruduction

In this work the position of the Simav Graben has been studied using geophysical data by applying 2D, 3D inversion and edge detection techniques. It was important to study if the techniques used in the field had any limitations or expansions and to know if they are general or site specific. As is the case in every discipline and under related disciplines, general and site specific solution relations are interconnected with each other.

The purpose of this study is to have a new 2nd and 3rd dimensional outlook to the Simav half graben and to the faults bordering the graben by applying geophysical techniques.

Bedrock image of the graben, image of the upper crust/lower crust interface,and the corner structure which developed as a result of intersection of the Simav and Naşa Fault Zones has been identified after applying the data processing stages. All of the processes were aimed at gaining the maximum data from the potential field maps and to work out physical parameters of the geology in the maps.

In the previous work; 2nd vertical derivative of the analytic signal (Hsu et al. 1996), horizontal derivative of the 'tilt angle' (Verdusco et al. 2004), 'hyperbolic tilt angle' and 2nd vertical derivative of the 'tilt angle' Cooper and Cowan (2004) methods have been used in the edge zone detection processes.

Ansari and Alamdar (2011) proposed the 'ASTA' technique as a new edge detection method. Original codes were written with the 'Matlab program' and were applied to the synthetic model data. Edge detection processes have been used in the Potensoft data processing software developed by Arısoy and Dikmen (2011). The processing menu does not include an ASTA module. The ASTA module was produced by modifying the program batch from the software and was added to the software menu and has so been used in this study.

As the 'tilt angle' acted like secondary potential, boundaries of the structures became clear so analytic signal relations and variations could be used to study the structures. Later on it passed from the phase filter to the derivative filter. So when 'tilt angle' and analytic signal processes have been applied

* Corresponding author : toker.ertan@gmail.com

separately, it was found out that developing negative signal/noise ratio have improved and corner sensitivities of the prism like model structures have been kept. Horizontal derivatives detecting edge boundaries, vertical derivatives localizing the anomaly and analytic signals giving high values at the structure are important contributions. Using the 'Tilt angle' method it was found out that with increasing depth blurring of the edge boundaries is no longer a problem, corner structures are kept and selectable edge zones are detectable.

2. Material and method

Following the introduction of edge detection technique, 'ASTA' components (analytic signal, tilt angle), comparison of the method with the other edge detection techniques have been made in this study. Edge detection and inversion methods have been applied to the field data of Demirbaş and Uslu (1986) and results have been critically discussed.

2.1. Analytic signal and Tilt angle:

Analytic signal:

Analytic signal 'M', Gravity or Magnetic potential field is given as;

$$AS(x,z) = \partial M / \partial x + i\partial M / \partial z \qquad (1)$$

Amplitude of the analytic signal is;

$$|AS(Z)| = ((\partial M / \partial x)^2 + (\partial M / \partial z)^2)^{1/2} \qquad (2)$$

3D Analytic Signal Theory:

It is easy to produce the analytic signal by computing the derivatives of the magnetic anomaly. Two dimensional Fourier transform pair applying as follows:

$$g(k_x, k_y) = F[f(x,y)] = \iint f(x,y) \, e^{-i(k_x x + k_y y)} \, dx, dy \qquad (3)$$

$$f(k_x, k_y) = F^{-1}[g(k_x, k_y)]$$

$$(\text{Equation 3}) = 1/4\pi^2 \iint g(k_x, k_y) \, k_x, k_y \, dk_x, dk_y$$

If the (k_x) and (k_y) are representing the wave numbers in x and y direction respectively, horizontal and vertical derivatives in the wave number domain by Fourier transform of the M magnetic potential, as well as the different derivative relations, could be determine by using the Eq. 3 (Roest et al., 1982).

If , $\hat{\mathbf{x}}$, $\hat{\mathbf{y}}$ and $\hat{z}$ are accepted as the unit vectors, 3D anayltic signal would be expressed as follows:

$$AS(x,z) = (\partial M / \partial x) \, \hat{\mathbf{x}} + (\partial M / \partial y) \, \hat{\mathbf{y}} + i(\partial M / \partial z) \, \hat{z} \qquad (4)$$

Passing through real and complex expressions in Hilbert transform pair from the Eq.4:

As the Fourier gradient in frequence domain:

$$\check{r}*F[A(x,y)] = \hat{h}*\nabla F[M] + i\hat{z}*\nabla F[M] \qquad (5)$$

The ∇ is the gradient operator in frequency domain.

If the operators are accepted as follows:

$$(ik_x \, \hat{\mathbf{x}} + ik_y \, \hat{\mathbf{y}} + |k| \, \hat{z}); \, \check{r} = \hat{\mathbf{x}} + \hat{\mathbf{y}} + \hat{z} \text{ ve } \hat{h} = \hat{\mathbf{x}} + \hat{\mathbf{y}}$$

considering the horizontal and vertical gradient relations of the potential, the real part of the Eq.5 represent the horizontal derivative whereas the complex part represents the vertical derivative (Pedersen, 1989).

$$\hat{h}*\nabla F[M] = i\hat{h}*\mathbf{k}F[M] = i((\hat{h}.\mathbf{k})/ |\mathbf{k}|)*|k| F[M]$$

$$=i((\hat{h}.\mathbf{k})/ |\mathbf{k}|)) * \hat{z}*\nabla F[M] \qquad (6)$$

The relationship between the horizontal and vertical derivative is the Hilbert transform operator in frequence domain $|[(\hat{h}.\mathbf{k})/ |\mathbf{k}|)]$ (Roest vd., 1982).

3D automatic interpretation of the grid data represents the 2D amplitude function and this function also represents the absolute value of Eq. 2 given by Nabignan (1972, 1974). In this case, this equation evolved as follows:

$$|AS(x,z)| = ((\partial M/\partial x)^2 + (\partial M/\partial y)^2 + (\partial M/\partial z)^2)^{1/2} \qquad (7)$$

This is the 3D analytic signal function. Analytic signal value (Eq.7) is maximum in the edge zones of the geological structures.

Because of the derivatives the places where there have been most changes are marked with strongest amplitude. In this statement it shows that origin of the structure becomes prominent. When multiple structures have been reduced down to original mass then as they become geological structural boundaries then they cannot be detailed any further (Ansari and Alamdar, 2011).

Tilt Angle:

In the edge zone detections Tilt angle is defined as one of the basic phase filters. Miller and Singh (1994) are the workers who discovered and used this filter. 'Arctan' of the ratio of the vertical derivative to the amplitude of the total horizontal derivative gives the tilt angle.

$$\text{Tilt=Arctan } (\partial M/\partial z) \ / \ [(\partial M/\partial x)^2+(\partial M/\partial y)^2)^{1/2} \quad (8)$$

Tilt angle acquires positive values (+90) on the original structure or nearby. When it is moved away from above the mass it first approaches to zero, then passes to negative values (-90) and it extends as a band in between negative and positive anomalies. Zero values indicate the edge zones. In between the anomaly contours, half distance between the $-\pi/4$ and $\pi/4$ contours is equal to the depth of the upper surface of the structure boundary (Salem et al, 2007). Figure 1 shows schematic view of tilt angle and the components.

2.2. Asta

In using the 'Tilt angle' method there may be some problems related to the study of the edge detection of deep seated structures. As there have not been any vertical variation measurements taken, in any the all of the determination studies carried out on the surface, vertical variation is determined with potential field strength. This inevitability is a problem in the vertical derivative. In the study area for the

masses present in various depths in the edge boundary transitions, the edge boundaries of the masses cannot be seen clear and sharp as they are needed to be.

In the regional studies, size of the field and multiple structures in it all appear in a narrow part in the data processing stages and features stand very close to one another making this interpretation of the field data becomes difficult. Vertical component ($\partial T/\partial z$) represents variation on the original tilt at depth. With the tilt angle the boundaries of the mass becomes known and depth effect of it is registered in the analytic signal. When analytical signal is used together with the tilt angle method then some features will appear more clearly.

In the equation 4 when 'T' tilt angle is written in place of 'M' potential

$$|AS(Z)| = ((\partial T/\partial x)^2 + (\partial T/\partial y)^2+ (\partial T/\partial z)^2)^{1/2} \quad (9)$$

equation is obtained. This is 'ASTA' equation, producing analytical signal from the tilt angle.

2.3. Derivative filters, phase filters and *asta* module used in the edge definitions

Arısoy and Dikmen (2011) prepared software for 'Potensoft'. It is for 3 rectangle prisms at 0-5 km depth (Figure 2); magnetic field effect (model grid) and model sensitivities of other edge definition methods have been studied. For this purpose in the order of;
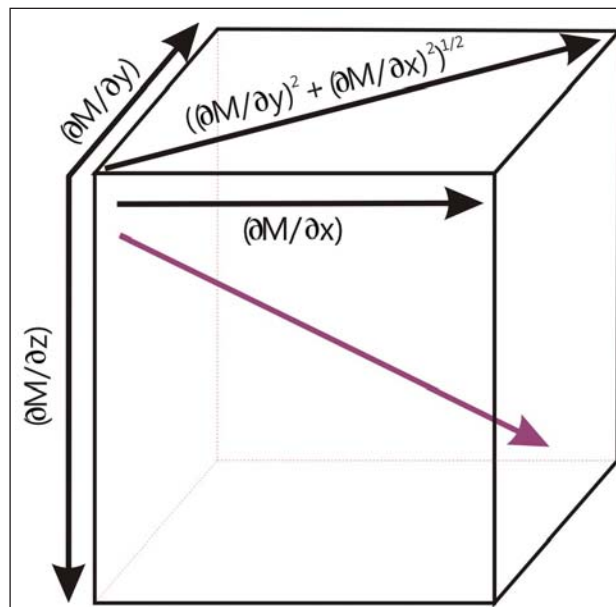

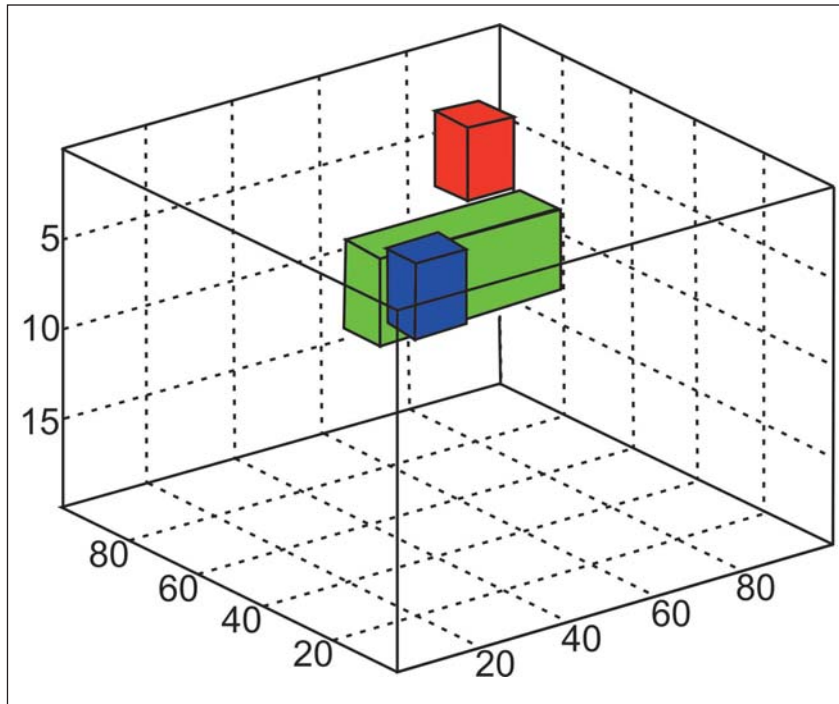Figure 1- Schematic view of the 'Tilt angle' components.

Figure 2- 3 dimensional model view (Arsoy and Dikmen, 2011).

(a) Model grid, (b) Horizontal gradient, (c) Analytical signal, (d) Tilt angle, (e) Tilt derivative, (f) Theta map, (g) Hyperbolic tangent (has not been pushed forward (?), and (h) *ASTA* (Tilt angle based analytic signal).

By using data processing, results have been correlated with each other. ASTA module is attached to the interface of the 'Potensoft' package program (Arısoy and Dikmen, 2011) and is present in the menu (Figure 3).

In general derivative filters are based on the calculations of the 1st and 2nd derivatives of the horizontal (along x and y) and vertical (along z) data. Analytic signal and horizontal gradient could be given as examples for the derivative filters. On the other hand phase filters are the angular greatness obtained from the base of the ratio of vertical derivative and the horizontal derivative angle. Hyperbolic tangent method can be given as an example. On the other hand the *ASTA* method is a mix edge sensing technique results from the derivation of 'till' greatness.

Figure 4 shows views of the 3 prisms produced with the edge definition methods.

2.4. Comparison of model answers

1) In Figure 4 model images in a, d, f and g show that anomaly fields has curvature expansions. Prism edges are not sharp and contour transitions are not clear. The four colours used (yellow, red, blue, green) show various transitions, detection of structures is problematical. Long edges of the rectangle prism in the middle have four coloured parallel transitions. This creates doubts on which could be the real edge. Distribution of the contours and colour shades may be misunderstood as structural complexity.

Figure 3- *ASTA* module view of the model grid attached to the graphic interface.

a) Model Grid

b) Horizontal Gradient

c) Analytic Signal

d) Tilt Angle

e) Tilt Derivative

f) Theta Image
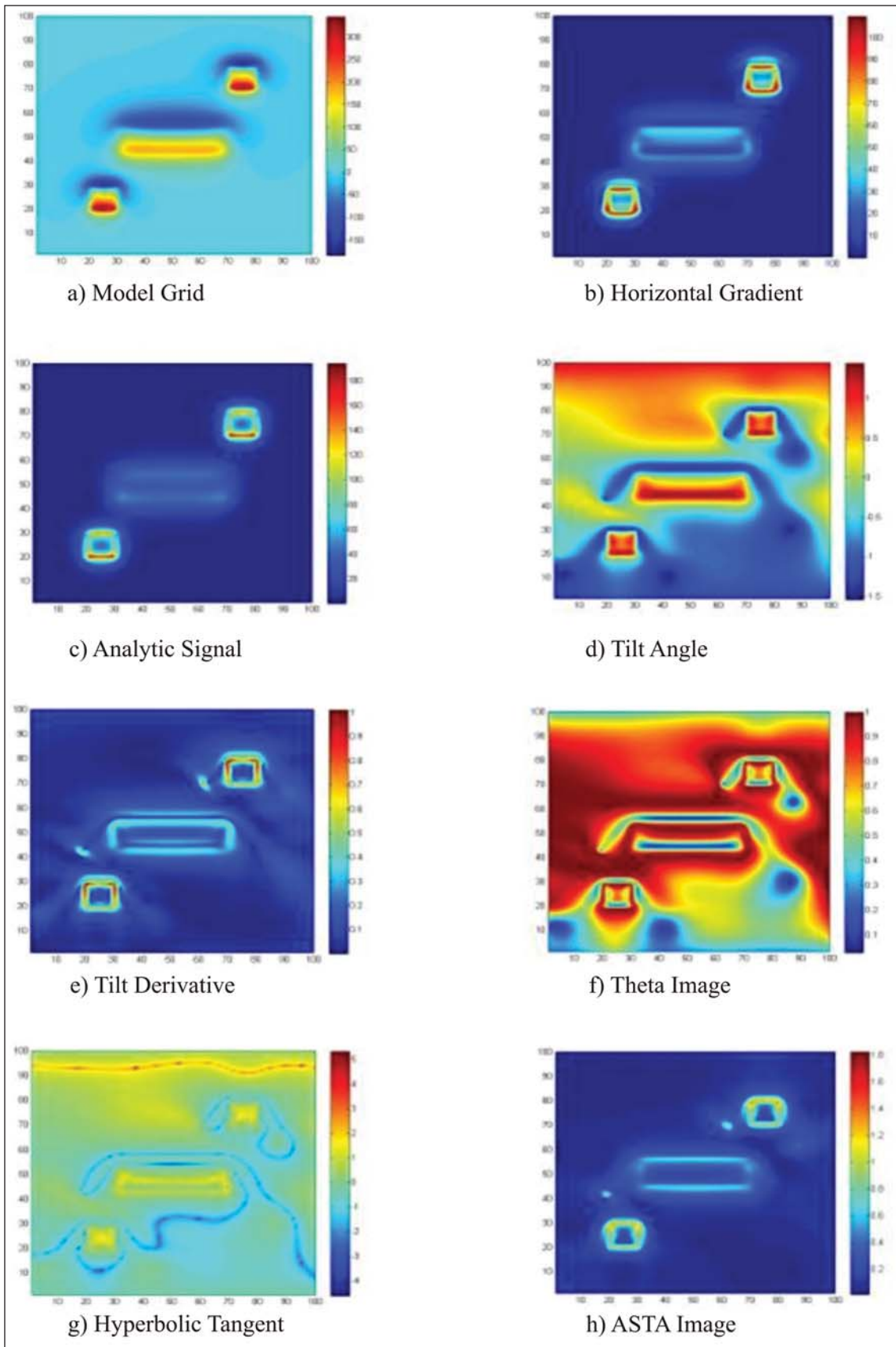
g) Hyperbolic Tangent

h) ASTA Image

Figure 4- Model answers for edge definition.

2) In Figure 4, image (b) is quite clear but there are contour accumulations on the top of the cubes and upper edges are narrower. Upper long edge of the rectangle prism in the middle appears to have thickened more so than it should.

3) In Figure 4, image in (c) is clearer than it is in (b) but the rectangle prism in the middle is not clearly visible.

4) In Figure 4, in the image (e), image of the tilt angle indicates that structures are geometric but contour accumulations and particularly repeated edge images along the long edges of the rectangle prism makes it difficult to understand the model.

5) In Figure 4, in image (h) in the *ASTA* image, although there are some small (local) contour accumulations some edge like with equal thickness geometric linear edge transitions, here with less noise and detectable upper prism images have been obtained here.

6) In figure 4, in image (h) the analytic signal obtained from the tilt angle is seen. The long rectangle prism in the middle has sharp edges and structures are visible. Among the methods shown in figure 4, only *ASTA* is a combination. But the analytic signal conducted following tilt angle application is not same as with *ASTA*.

Although conducting repeated edge sensing methods conducted showed some sharp edges in the structures but the images of the edges of the rectangle

prism in the middle are still not sharp. In figure 5 and figure 6, it shows 2nd vertical derivative applied following analytic signal by Hsu et al., (1996) and 2nd vertical derivative applied following tilt angle by Cooper and Cowan (2004).

In the lower left side and in the upper right side in figure 5 although the effect of the prism edges appear sharp but the edges of the long prismatic structure in the middle is not clear. In figure 6, despite colour interferences the edges of the three prisms are visible but are not sharp. Although there are more data processing and processing time in the second derivative combinations but still contrast and signals are weak, images are not sharp (Figures 5 and 6).

3. Simav Fault and Geological Position of Simav Half Graben:

Aegean graben system including the Simav Graben was concerned by many authors since 60'ies (Arpat and Bingöl, 1969). In North-western Turkey extensions of NE-SW extending Demirci, Selend, and Gördes basins are limited by the Simav fault zone. Here E-W extending Pliocene (?)- Quaternary subsidence zone is known as the Simav Graben (Şaroğlu et al., 2002), (Figure 7a). Seyitoğlu et al., (1997) studied the fault mechanisms and concluded that Simav Graben fault was an active geometric listric fault zone. According to this author, this structure was developed as a result of N-S running extensional fault zone which effected Aegean region in Late Oligocene – Early Miocene. Doğan and Emre (2006) say that depending upon the geomorphologic
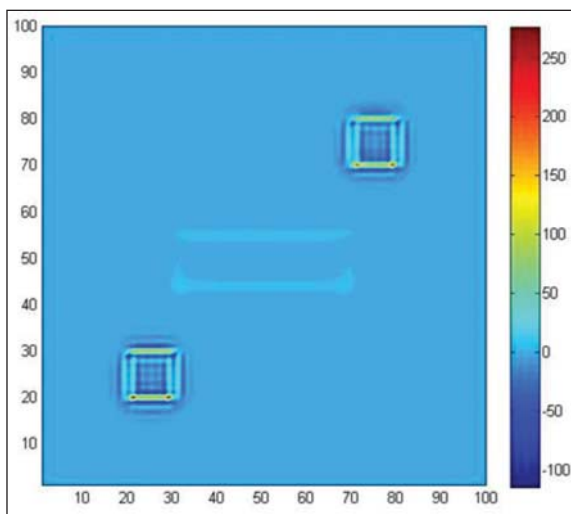

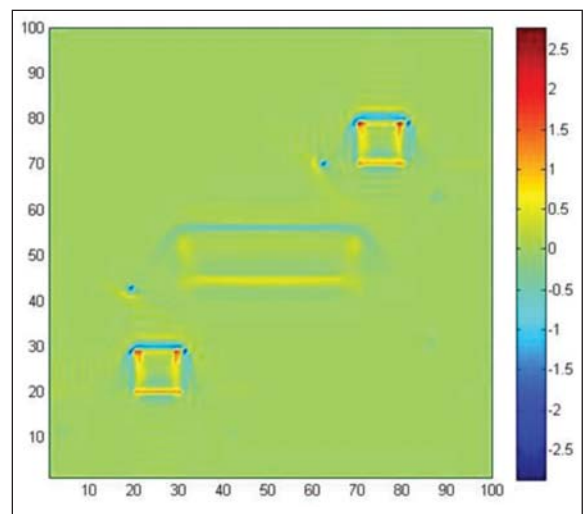Figure 5- 2nd vertical derivative of the analytic signal;

Figure 6- 2nd vertical derivative of the Tilt angle

findings the plain base where Simav lake is located has subsided during the last 10000 years as a result of earthquakes. According to another view of Doğan and Emre (2006) there is a 205 km long strike slip fault which joins to the Gelenbe fault at the western end of the Simav fault zone and to the East end of the Sultandağı fault zone.

The Northern end of the graben is bound by Naşa Fault Zone which consists of numbers of normal faults and further north by Emet (Kütahya) fault (Emre et al., 2013). According to Emre et al. (2013) Simav plain is the largest structural subsidence basin in the Simav fault zone. It is a basin developed on the right step-over between Simav and Şaphane faults.

The regional tectonic map and position of the study area is given in figures 7a and 7b respectively.

Emre et al. (2013) says that in the earthquake stricken region strike slip faults caused the recent tectonic deformations. Main earthquake producing tectonic features in the region are NW-SE running right lateral Simav fault and the Naşa Fault Zone which is made of series of NW-SE running faults (with 55° - 65° west dipping) (Figure 7b). It is still argued whether Simav fault is a listric geometric normal fault (Seyitoğlu et al., 1999) or right lateral, strike slip regional normal fault (Emre et al., 2013).

In the literature the relationship of the Simav fault with the Menderes massif is extensively discussed. According to Gessner et al. (2013) the fault is within the Menderes massif (Figure 8). On the other hand, according to Koralay (2011) the Simav Fault does not have a boundary relation with the Menderes massif (Figure 9).
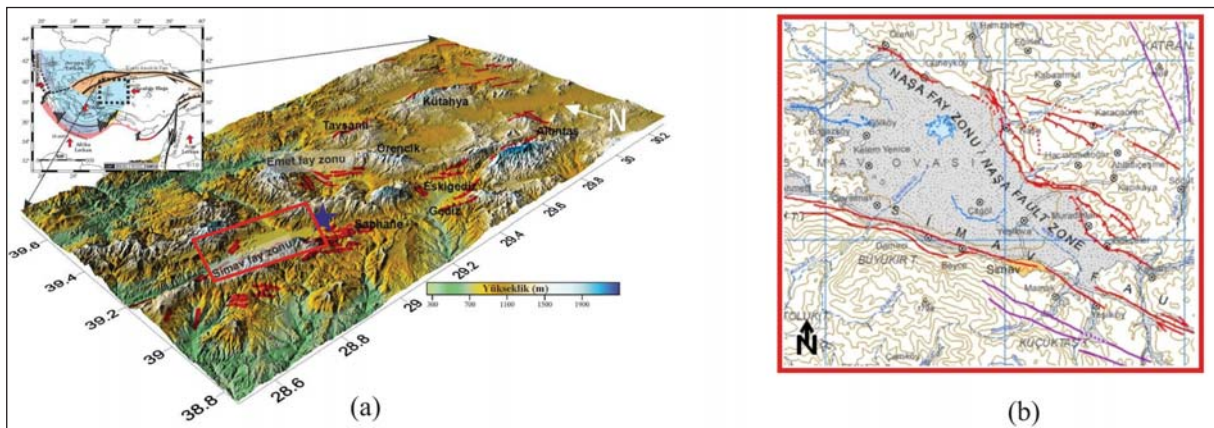

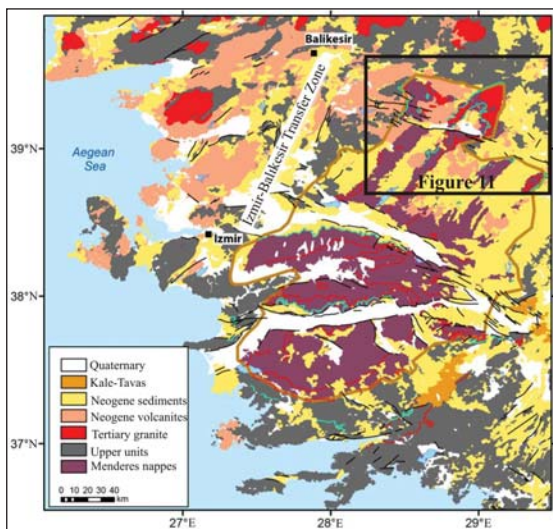Figure 7- a) Regional tectonic map (Şaroğlu et al., 2002); b) Study area.

Figure 8- Limits of the Menders Massif (from simplified map of MTA, 2002 of Gessner, et al., 2013).
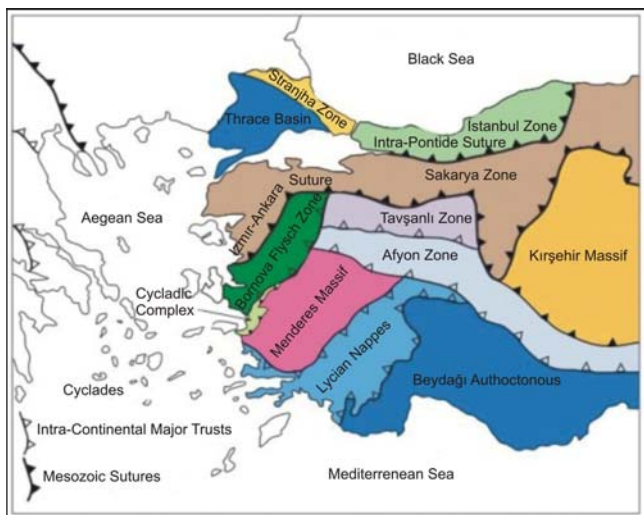
Figure 9- Simplified regional tectonic map (Okay et al., 1996; from Koralay et al., 2011).
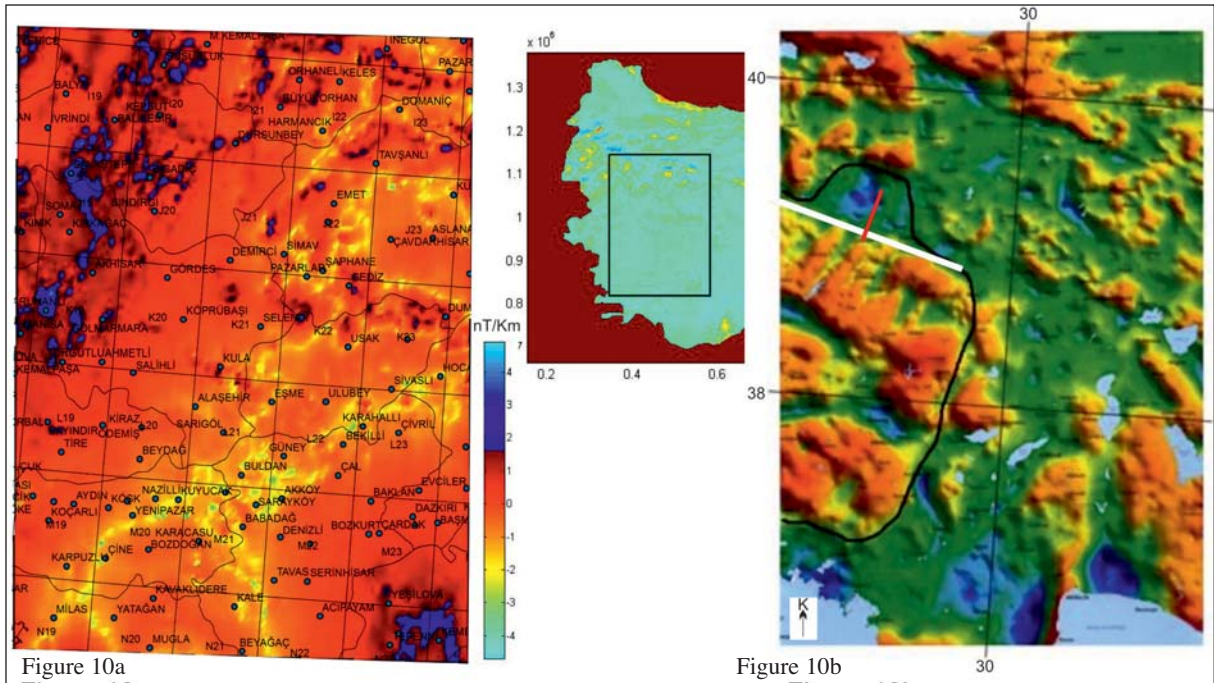
Figure 10- a- Northern boundary of the Menderes massif, based on the air borne magnetic data b- Gravity residual izostasy map; white line: Simav Fault; red line: cross section line in the figure 12 (Modified from MTA, 2012).

Air borne magnetic data and regional gravimetric data suggest that Menderes massif has tectonic border zone (Figures 10a and b). Magnetic susceptibility in the massif area has largely diminished. But in the neighboured there appear to be present a 'puzzle void' with magnetic susceptibility. It appears that Simav fault and the subsidence zone to the North are within the magnetic and gravity field.

To the north of the magnetic map there is a group of rocks with similar origin and having similar physical properties. When edge sensing technique is applied to this group of rocks there appears a structure along a 'cloth hanger' like line (black line) which may be defined as a physical transition. The black line may possibly be defining the northern boundary of the massif (Figure 10b). Menderes massif forms a tectonic unit and physical changes along the borders of this unit are reflected as partly (in the north) geophysical anomaly on the maps.

In Figure 11 blue line is marked as a detachment fault (Gessner et al., 2013). A scientist working in the Simav basin may consider that the units in the basin have moved forward along the Simav fault and the basement block in the north has moved eastwards (Figure 11).
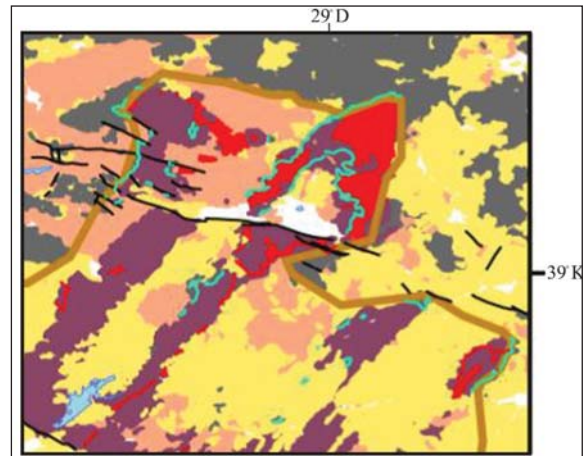

Figure 11- Northern boundaries of the Menderes massif, Eğrigöz granitoid and the detachment faults (after Gessner et al., 2013).

This movement may appear contradicting with the Northwest-Southeast movement of the graben systems, but both are in accord with the gravity data. If cross sections are taken along Northwest - Southeast and Northeast –Southwest directions on the gravity maps, one could see that these cross sections are in accord with the graben model and fault (normal fault) definitions.

4. 2D Host rock image of the Simav basin

Theoretical model of the Simav Graben and the real gravity profile on it is given in figure 12. In this profile the edge of the topographically high block in the Southwest is marked with some faults. Step faults in the Northeast are defining Naşa Fault Zones.

In figure 12, it shows that in the upper part gravity value drops from about -55 mgal down to -65 mgal. The anomaly is becoming almost horizontal in the graben, then (probably from the effect of basalts) it increases towards the other end of the graben where there are normal faults and ending with parallel anomaly oscillations. It indicates that the units in the east are denser than the filled up material in the graben. Anomaly values in the graphic are the measured gravity values. Host rock gravity values produced by two dimension inversion solution from this profile are seen as 'iteration 27' values in table 1.
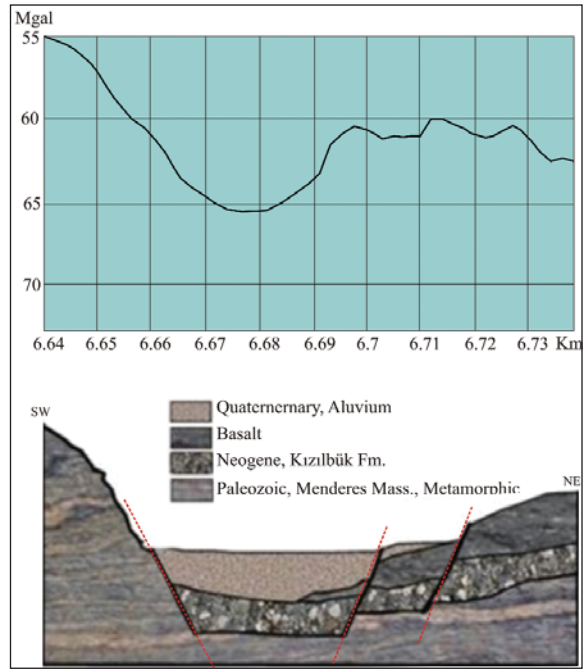

Figure 12- Conceptual model and measured gravity anomaly.

Table 1- '27 iteration' values of inversion solution.

27th Iteration						
Distance	Measured Gravity (mgal)	Depth	X1	X2	Gravity value (mgal)	Calculated Gravity (mgal)
664.5	-65.06	0.05101	-0.25	0.25	-1	-1
665	-65.67	0.0847	0.25	0.75	-1.6099	-1.6099
665.5	-66.68	0.14845	0.75	1.25	-2.62	-2.6199
666	-68.49	0.29636	1.25	1.75	-4.4299	-4.4299
666.5	-69.69	0.3841	1.75	2.25	-5.6299	-5.63
667	-70.77	0.47763	2.25	2.75	-6.7099	-6.7099
667.5	-72.85	0.79225	2.75	3.25	-8.7899	-8.7867
668	-74.66	0.95224	3.25	3.75	-10.599	-10.608
668.5	-75.67	0.94065	3.75	4.25	-11.61	-11.613
669	-75.67	0.79054	4.25	4.75	-11.61	-11.602
669.5	-75.47	0.76628	4.75	5.25	-11.409	-11.401
670	-73.67	0.44944	5.25	5.75	-9.61	-9.6164
670.5	-73.07	0.52456	5.75	6.25	-9.0099	-9.0101
671	-71.26	0.30696	6.25	6.75	-7.2	-7.2002
671.5	-70.53	0.32433	6.75	7.25	-6.4699	-6.4697
672	-70.6	036751	7.25	7.75	-6.5399	-6.5403
672.5	-71.2	0.45116	7.75	8.25	-7.14	-7.1399
673	-70.87	0.37307	8.25	8.75	-6.81	-6.8101
673.5	-71.07	0.42863	8.75	9.25	-7.0099	-7.0098
674	-69.74	0.25848	9.25	9.75	-5.6799	-5.6801
674.5	-70.34	0.38892	9.75	10.25	-6.28	-6.2799
675	-71.15	0.46693	10.25	10.75	-7.09	-7.0901
675.5	-70.62	0.35118	10.75	11.25	-6.56	-6.5598
676	-70.48	0.37025	11.25	11.75	-6.42	-6.42
676.5	-71.09	0.45807	11.75	12.25	-7.03	-7.0301
677	-72.5	0.65621	12.25	12.75	-8.4399	-8.4392
677.5	-72.37	0.49362	12.75	13.25	-8.31	-8.3114
678	-72.43	0.53922	13.25	13.75	-8.37	-8.3675
678.5	-72.77	0.58586	13.75	14.25	-8.7099	-8.7126

In the Eastern part of the basin along the Southwest-Northeast profile, while southern flank is descending with high angle, northern flank is going up with low angle (Figure 13).

Previously magneto telluric studies were carried out in the field. From the magneto telluric studies two dimensional inverse solution gravity values were found out. Figure 14 shows gravity profile selected to be close to the two dimensional inverse solution values. On this gravity profile (Figure 14) dotted red line and continuous line show agreements with the positions of the main fault zones.
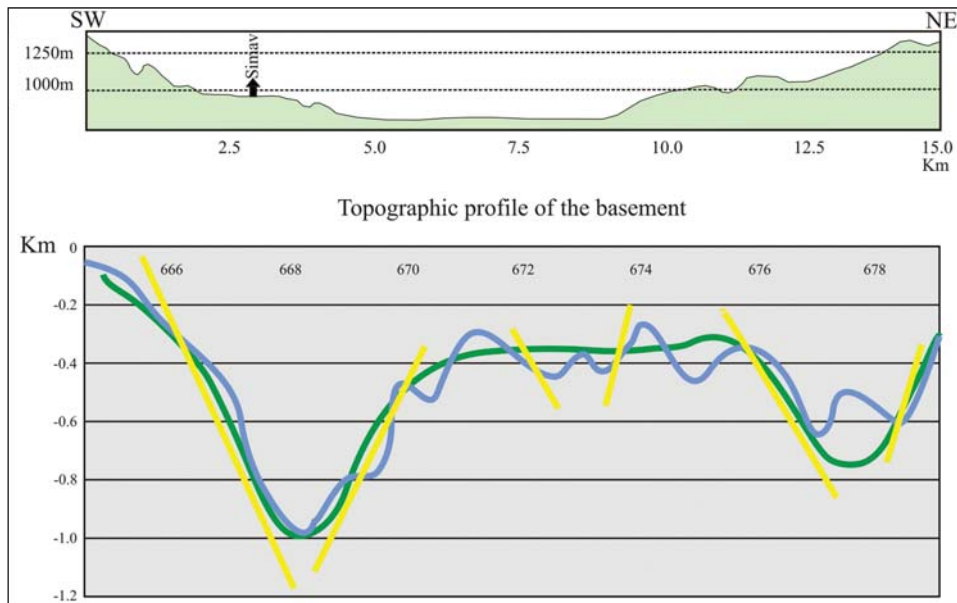
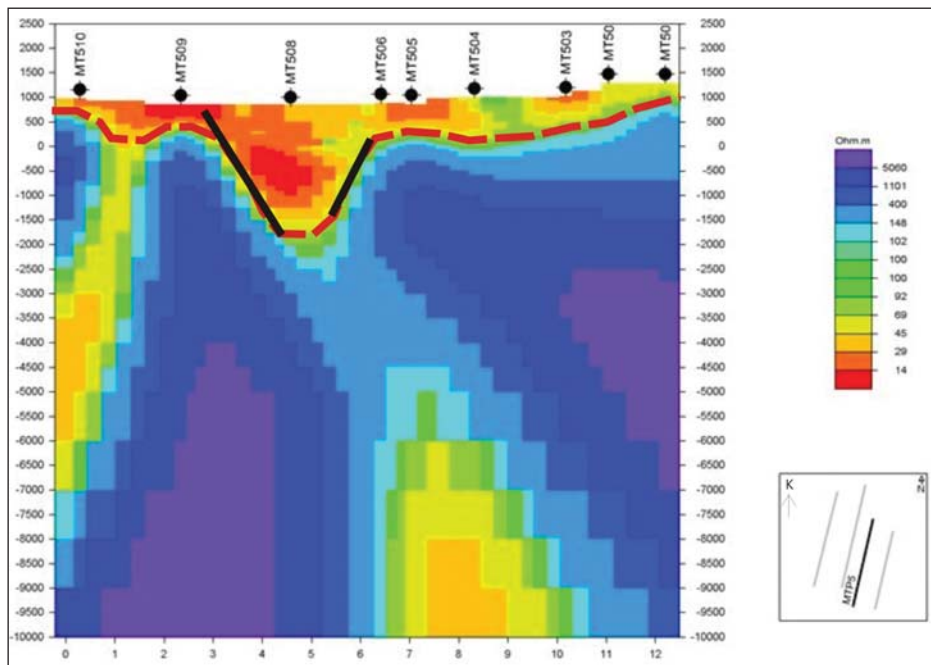Figure 13- Host rock image under the gravity section (Blue line: host rock; yellow line: faults).

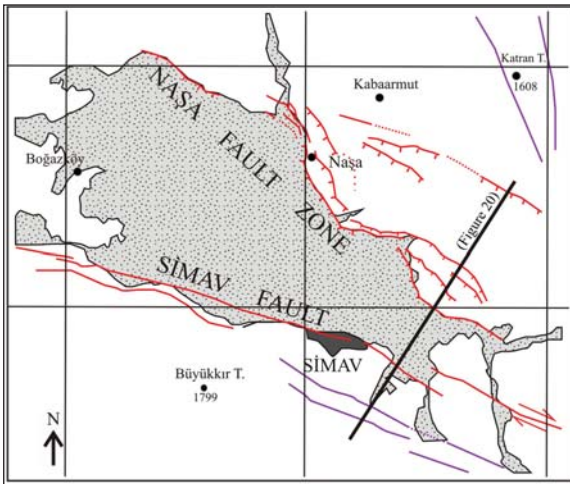Figure 14- Closely positioned, 2D inverse solution profile view (Kılıç, 2010).

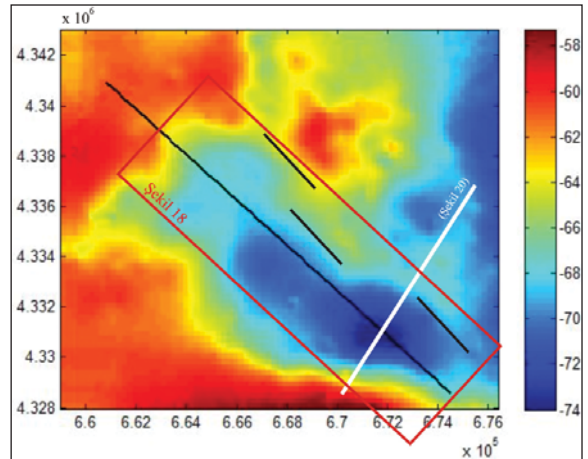Figure 15- Updated active fault map (Emre et al., 2012);

Figure 16- Bouguer gravity map of the study area and selected cross section (white line: Figure 20); red rectangle: area of the figure 18 (data from Demirbaş and Uslu, 1986).

The triangular shape structure becomes narrower towards East (where gneisses are). It's southern boundary has a distinct gravity transition. In the North, the Naşa Fault Zone transitions has been well marked on the active tectonic map and can be seen on the gravity map (Figure 15, 16).

Position and shape of the graben shown in the updated active fault map (Emre et al., 2013) is in agreement with the gravity map. In the gravity map granitoids have – (60-64) mgal values, gneisses along the lower edge of the graben have – (72-74) mgal values. Blue coloured parts in figure 16 reflects gravity effect of the Quaternary in fills.

5. Gravity edge definition technique and 3D analysis

To be able to study deep and shallow structures, various different processes are needed. Studying the edge zone effects of shallow structures, derivative and phase filters give satisfactory results. On the other hand while studying the edge sensing of deep structures some problems related to vertical derivative effects may arise. These problems have been tried to be solved by upward analytic continuation and vertical derivative applications.

Analytic signal was applied to 2 dimensional structures by Nabighian (1972). Since then various computer programmes have been developed. Nowadays package software's have 'edge detection' modules. If analytic signal is the result of subtraction of absolute value of complex Hilbert transforms from

the function then highest values are expected to be at contour transitions.

It is known that analytic signal technique is not sensitive to the structure corners. Following horizontal gradient applications, analytic signal derived from the tilt angle becomes sensitive to the structure corners (Figure 17a, b). When the concept of analytic signal is thought to be source rock mass effect; to be able to see the maximums along a line, then horizontal gradient would be needed. Following removal of surface effects with upward analytic continuation applications, horizontal gradient and ASTA have been applied (Figure 17b). In figure 18, a 3D analysis derived from inverse solution of quadratic density function with constant -0.7 gr/cm^3 specific gravity contrast is given. This view could be characterized as upper crust interface. In this view southern edge is leaping and making a bend to yellow coloured contour transition. In the program calculations a positive value is estimated, because of this depths are positive and are at interface topography position.

Simav Graben appears as a subsidence area in the gravity inversion. In the red dotted marked area where Simav fault cuts through the graben there is a subsidence like feature but this feature does not have any surface signature (Figure 18).

6. Findings

Two and 3-dimensional gravity processes have been obtained by using programmes with various
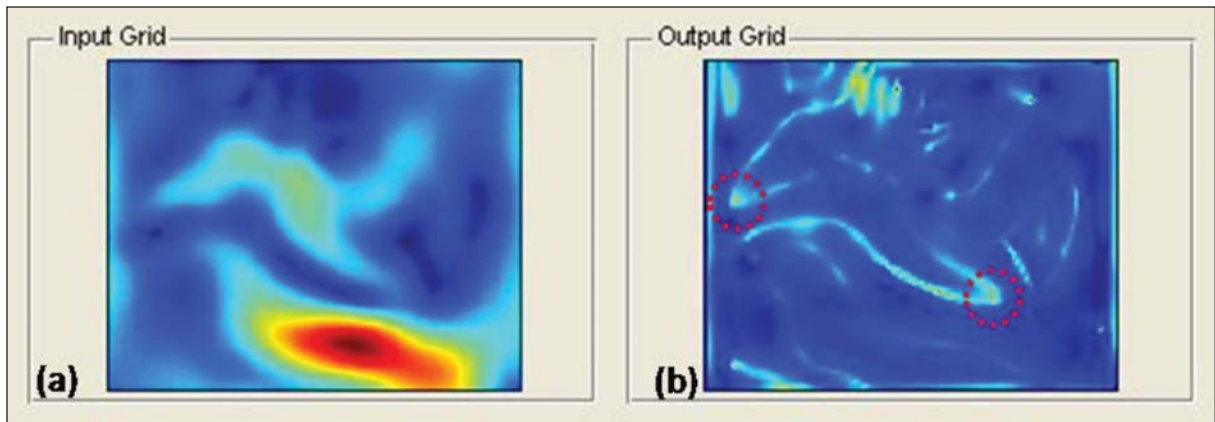
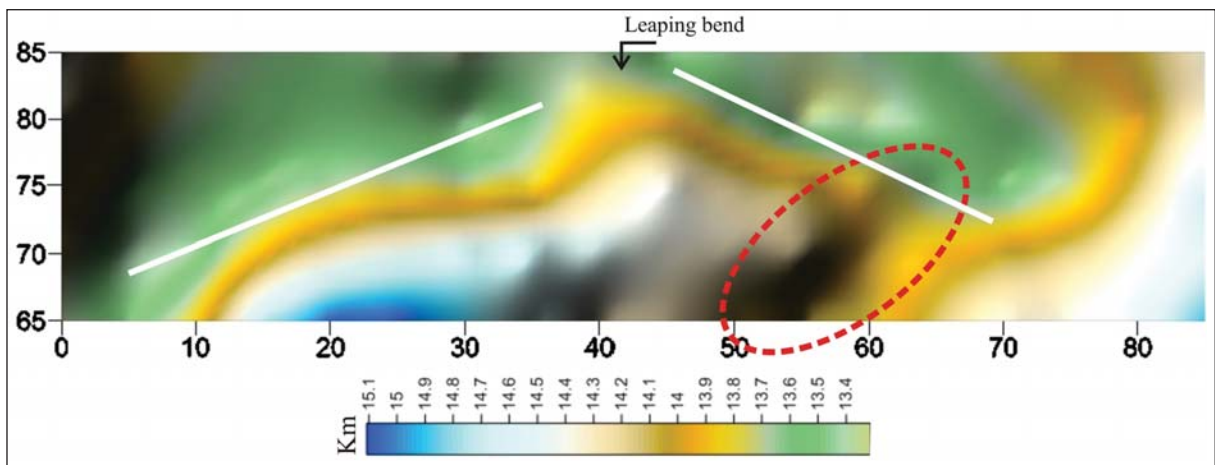Figure 17- a) Horizontal gradient view; b) Horizontal gradient + ASTA

Figure 18- Basin depth map based on the 3D analysis of the 3D Bouguer gravity map (see figure 16 for location).

different techniques. Two-dimensional edge definitions, gravity data processings, Matlab process software has been made by using Potensoft developed by Arısoy and Dikmen (2011). Three-dimensional analyses have been made by using Fortran (Goncalves, 2006). In this study iterative 3-dimensional inversion have been used the foundations for this method were laid down by Cordel and Henderson (1968). This program also includes quadratic gravity function preferred by Bhaskara and Ramesh (1991).

ASTA as edge sensing method has been tried and model sensitivity and solution performance for deep structures have been studied. But 'ASTA' has not been applied directly to the raw data. For the deep structures, upward analytic continuation, low-pass filters and horizontal gradient methods were applied before ASTA.

In 3D analysis, square data without coordinates are used and then program print out is designed with relative coordinates. In the program an algorithm with specific gravity distribution defined with a quadratic function is used and specific gravity contrast of the basin base forms interface geometry (Figure 18). Here it is advantageous to use the best representing function of the basin's base contrast. Although the program may provide facilities to define the basin's depths, in places where specific gravity differences are minimal at depths then iterative takings may vary. Defined base depth estimate may be used as a parameter to start the process.

The base of the basin is defined as low 'Vp' velocity and high 'b' value in the seismology profile of the crust joint research project package of Tubitak-MTA- University (Figure 19). In the profile where Simav is, there is a low velocity anomaly at 2-3 km depth with 3.3-3.7 km/s velocity. Study shows that
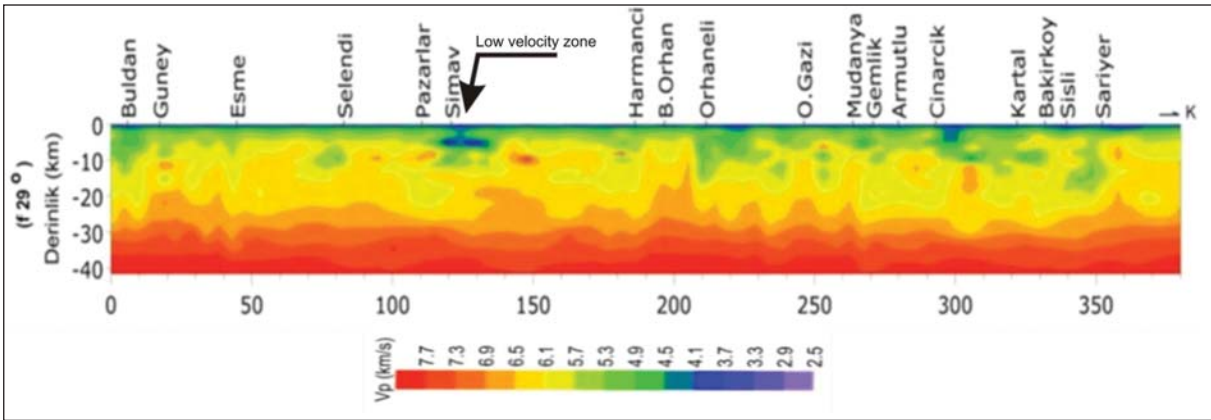
Figure 19- Seicmic velocity (Vp) section, blue area 3.3 km/s, low velocity zone (See figure 15 for location) (MTA, TÜBİTAK, C.Ü., A.Ü., 2012).

low velocity is related either to the in filled loose material or to the subsidence. High 'b' value reflects degree of compaction (Figure 19).

The edge of the basin in the south is bound by a normal fault with high dip angle. In the north the basin is bound by normal faults with lower dip angles. In Figure 18 there is a graben feature which has Simav fault in the south and Naşa Fault in the north. As it was the case for Büyük Menderes and Gediz grabens, here from the 2 dimensional inverse solution of the southwest-northeast gravity profile it shows that this graben is an asymmetric half graben developed in the north of Simav main fault..

A selected profile, subjected to 2D inversion solution indicates that near Simav there is a more undulated host rock base profile. On the surface the

host rock profile traverses Naşa Fault Zone. This is the part where earthquakes are quite frequent. As is the case in Gediz and Büyük Menderes grabens (Sarı, 2003) host rock profile here also dips eastwards (Figure 20).

The leaping coil as it is described by Doğan and Emre (2006) is clearly seen in the 3D deep gravity solutions and regional gravity data processing's with edge sensing's (Figure 21b). 13 to15 km seismologic depth limit seems rather adequate for gravity. In the south where the big fault is thought to have made a coil appears in accord with the 2 and 3 dimensional maps prepared by using the gravity data (Figure 21).

Red dotted lines mark the area where the fault made a coil in the map. Same lines also fit to the southern edge of the 2 dimensional images. In practice when ASTA is carefully applied some of the
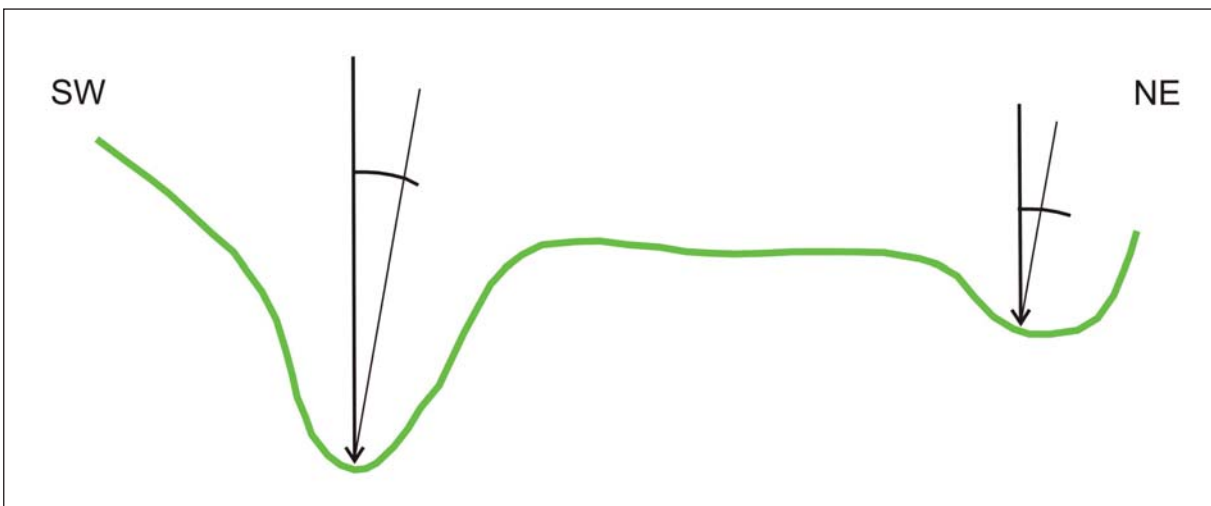

Figure 20- Asymmetric half graben model (see figure 16 for profile location).
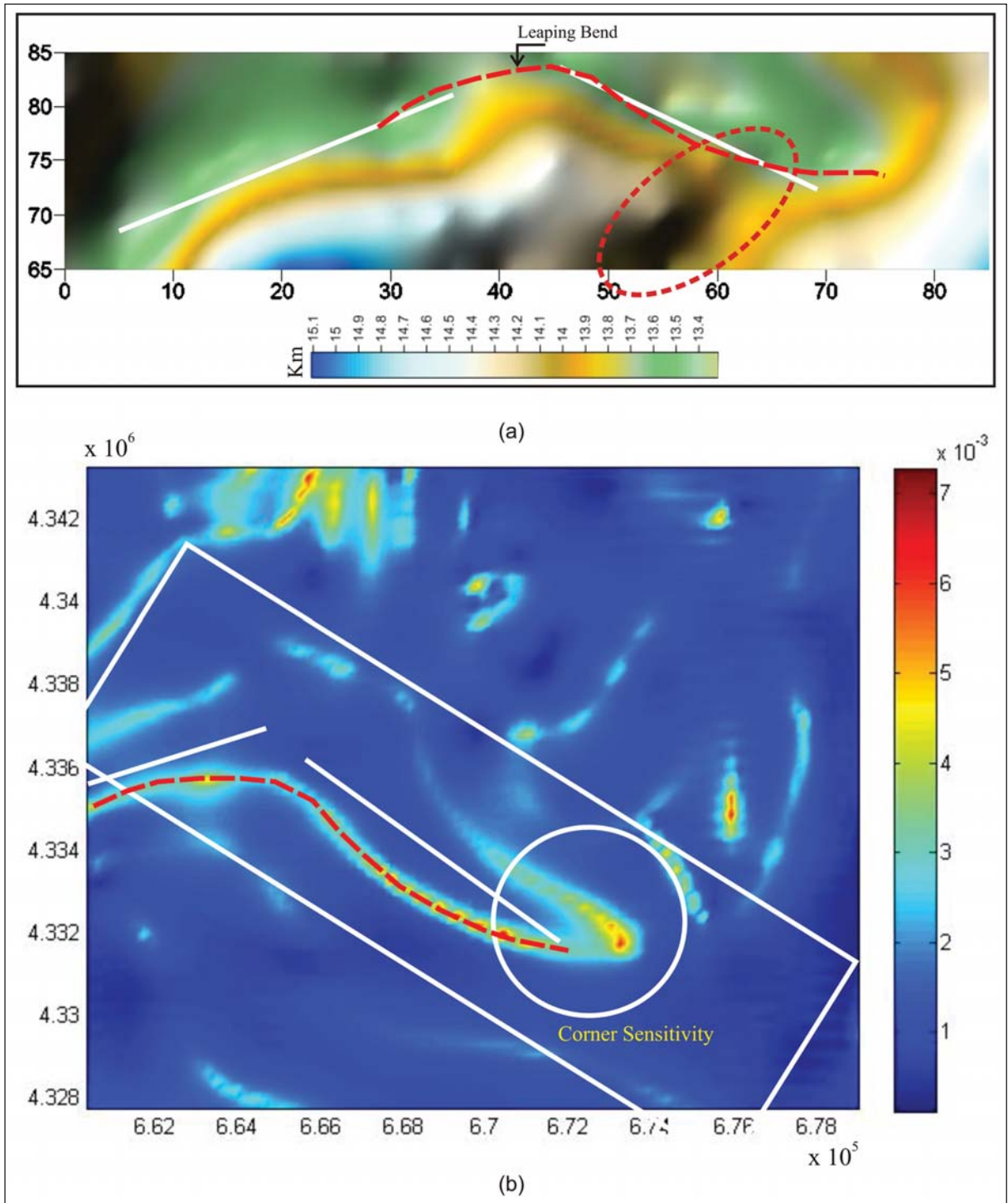
Figure 21- Joint field image of 2D and 3D solutions (White rectangle on figure 21b represent the map area of the figure 21a).

unwanted effects encountered in other edge sensing applications can be avoided. Yellow line (in the white coloured circle) shows that analytic signal could be recorded at the structure corners (Figure 21). Here below it is shown that 3 layered image is in accord with the edges (Figure 22). In the faults here Focal mechanism solutions indicate that the faults developed here are normal faults and had some strike slip component (Figure 23) (Bekler et al., 2011). It appears that the area where the earthquakes commonly occur coincide with the intersection of two faults on the surface and possibly intersection of the third fault at depth.

3D Basin depth interface model of the Simav Basin were produced after all the processes and studies writen above and presented in figure 24.

7. Discussion and Results

- Simav fault is about 205 km long. It is not appropriate to define this fault as a whole with a as a single character as some sections are with dominant component. For example it's part in the graben is normal fault with high dip angle (Figures 13 and 14). It is quite natural to see different characters in different parts of the fault. The part of the fault in the graben in places has strike slip components (Gessner et al., 2013).

- For paleo seismological studies multiple geophysics criteria should be used to locate where the trenches to be cut. It has been shown that rather than cutting the trenches on the surface expression of the fault, cutting in on the location where geophysics image suggests is much more informative.

- Gravity data indicate that graben in the south is a half graben (Figure 20). Simav fault in the graben is a normal fault. Edge sensing processes show that the Simav fault and intersection of the NW-SE running Naşa Fault, bordering the half graben, where there is a corner structure, coincides with the focal of many earthquakes (Figures 22 and 23). In some places host rocks at a depth of 1000-1200 m (Figure 13) and in accord with the seismology inversion presence of a upper crust interface topography at 13-15 km depths can be seen (Figure 19).

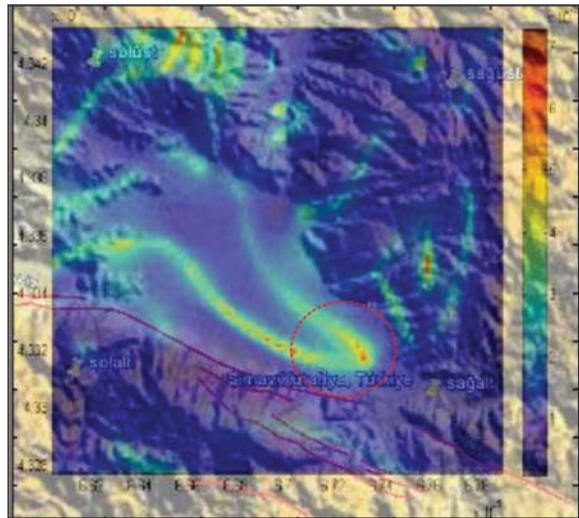- Numbers of earthquakes generated during the last two years relating to the faults in the Simav basin

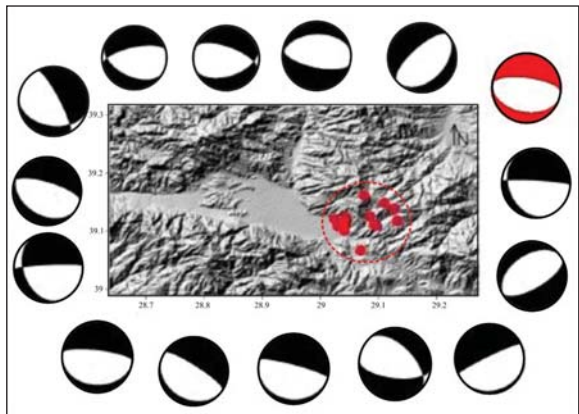Figure 22. 3 layered superimpozed image. Yellow lines edge zone sensing ASTA.

Figure 23- Moment tensore solutions. Red ball 19th May 2011, Mw=5.83 (Bekler et al., 2011);

shows that how much the area is tectonically active and how much the tension is high. Altınok et al., (2012) reports that studies on the 'Holocene activities of the Kütahya fault zone' show, the fault zone has the potential for producing earthquakes at 6.5 Magnitudes.

- Defining the deep part geometries of the deep seated faults in the region will provide more accuracy about locate and modelling the fault segment that would be activated. That is why, after using the 2D and 3D geophysical models in areas like the Simav region to understand the deep geometry would also provide more acurracy in geological modelling.

- 3D Basin depth interface model of the Simav Basin produced at first in this study in the light of the detail gravity data.
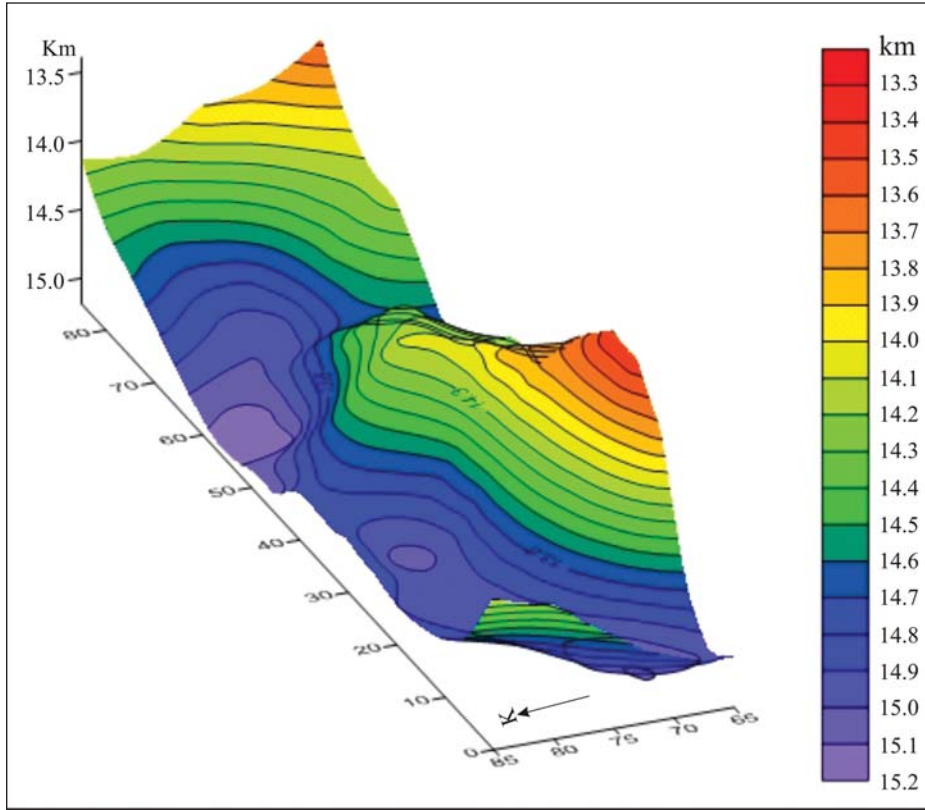
133

Figure 24- 3D Basin depth interface model of the Simav Basin.

References

Altınok, S., Karabacak, V.,Yalçıner, C.Ç., Bilgen, A.N., Altunel, E., Kıyak, N.G. 2012. Kütahya fay zonunun Holosen aktivitesi, *Türkiye Jeoloji Bülteni*, 55, 1.

Ansari A. H., Alamdar, K. 2011. A new edge detection method based on the analytic signal of tilt angle (*ASTA*) for magnetic and gravity anomalies, IJST A2: 81-88, *Iranian Journal of Science and Technology*.

Arısoy, M.Ö., Dikmen, Ü. 2011. Potensoft: MATLAB-based software for potential field data processing, modeling and mapping, *Computer and Geoscience*, 37, 7, s. 935 – 942.

Arpat, E., Bingöl, E.,1969. Ege bölgesi graben sisteminin gelişimi üzerine düşünceler, *Maden Tetkik ve Arama Dergisi,* 73, 1-9, Ankara.

Bhaskara, D., Ramesh, N. 1991. A fortran-77 Computer program for three-Dimensional Analysis of gravity anomalies with variable density contrast, *Computer and Geoscience*, 17, 5, s. 655-667.

Bekler, T., Demirci, A., Özden, S., Kalafat, D. 2011. Simav, Emet fay zonlarındaki optimum kaynak parametrelerinin analizi, 1. Türkiye Deprem Mühendisliği ve Sismoloji Konferansı, ODTÜ, ANKARA.

Cooper, G.R.J., Cowan, D.R. 2004. Filtering using variable order vertical derivatives. *Computer and Geoscience*, 30, 455-459.

Cordell, L., Henderson, R.G. 1968. Iterative three-dimensional solution of gravity anomaly data using a digital computer, *Geophysics*, 33, 596-601.

Demirbaş, Ş., Uslu A. 1984. Kütahya Simav Gravite Etüdü, *Maden Tetkik ve Arama Genel Müdürlüğü Rapor* No: 8136, Ankara (unpublished).

Doğan, A., Emre, Ö. 2006. Ege graben sisteminin kuzey sınırı: Sındırgı Sincanlı Fay Zonu, 59th.

Geological Congress of Turkey, Proceeding Books.

Emre, Ö., Duman, T.Y., Duman, Ş., Özalp, S. 2012. Türkiye diri fay haritası (yenilenmiş), *Maden Tetkik ve Arama Yayınları*, Ankara.

Gessner, K., Gallardo, L.A., Markwitz, W., Ring, U., Thomson, S.N. 2013. What caused the denudation of the Menderes massif: Rewiev of the crustal evaluation, lithosphere structure, and dynamic topograpy in soutwest Turkey. *Gondwana research*, 24/1, 243-274

Goncalves, W.J. 2006. Inversion gravimetrica 3d de la subcuenca de maturin Üniversidat Simon Bolivar proyekto de grado thesis.

Van Hinsbergen, J.J. 2010. A key extensional metamorphic complex rewieved and restored: The Menderes massif of western Turkey, *Earth Science Rewievs*, 102, 60– 76.

Hsu, S.K., Sibuet, J.C., Shyu, C.T., 1996. Depth to magnetic source using generalized analytic signal, *Geophysics*, 61, 373-386.

Kılıç, A.R., Kaya, C., 2010. Simav jeotermal sahasının manyetotellurik yöntemle araştırılması, Yer Elektrik Çalıştayı, Kastamonu.

Koralay, O. E., Candan, O., Akal, C., Dora, Ö., Chen, F., Satır, M., Oberhansli, R. 2011. Menderes masifindeki Pan-afrikan ve Triyas yaşlı metagranitoyitlerin jeolojisi ve jeokronolojisi, Batı Anadolu, Türkiye, *Maden Tetkik ve Arama Dergisi*, 142, 69-121.

Miller, H. G., Sing, V. 1994. Potential field tilt - A new concept for location of potential field sources: *Journal of Applied Geophysics*, 32, 213-217

MTA, TÜBİTAK, C.Ü., A.Ü., 2012. 105G145 No'lu Tübitak, Maden Tetkik ve Arama Genel Müdürlüğü, Sivas Cumhuriyet Üniversitesi, Ankara Üniversitesi İşbirliği Projesi, 2012. Kuzeybatı Anadolu Kabuk Yapısının Jeofizik Verilerle Araştırılması Projesi", 2008- 2012, Ankara (unpublished).

Nabighian, M.N. 1972. The analytic signal of two dimensional magnetic bodies with polygonal crossection: it's properties and use for automated anomaly interpretation, *Geophysics*, 37, 507-517.

Pedersen, L. B. 1989, Retations between horizontal and vertical gradients of potential fields Geophysics, 54, 662-663.

Roest, W. R., Verhoef, J., Pilkington, M. 1992. Magnetic Interpretation using the 3-D analytic Signal Geophysics, 1, 116-125, January 1992.

Salem, A., Williams, S., Fairhead, D., Ravat, D. V., Smith, R. 2007. Tilt-depth method: A simple depth estimation method using first-order magnetic derivatives: The Leading Edge, December, 1502-1505.

Sarı, C. 2003. Gravite verilerinin tekil değer ayrıştırma yöntemi ile ters çözümü ve Gediz ve Büyük Menderes grabenlerinin tortul kalınlıklarının saptanması, *DEÜ Mühendislik Fakültesi Fen ve Mühendislik Dergisi*, 5, 1.

Seyitoğlu, G. 1997. The Simav Graben: An example of young E-W trending structures in the late cenosoic extensional system of western Turkey. *Turkish Journal of Earth Science*, 6, 135-141, TÜBİTAK, Turkey.

Verdusco, B., Fairhead, J.D., Green, C.M. 2004. New insigth in to magnetic derivatives for structural mapping, *Leading Edge*, 23 (2), 116-119.